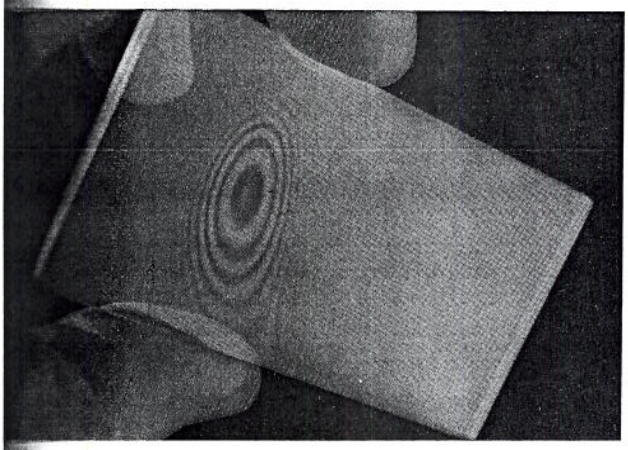

URE 9.25 Newton's rings with two microscope slides. (E. H.)

...e $R >> d$, this becomes

$$x^2 = 2Rd$$

...ume that we need only examine the first two reflected ...s E_{1r} and E_{2r}. The mth-order interference maximum will occur in the thin film when its thickness is in accord with the relationship

$$2n_f d_m = (m + \tfrac{1}{2})\lambda_0$$

The radius of the mth bright ring is therefore found by combining the last two expressions to yield

[bright ring] $$x_m = [(m + \tfrac{1}{2})\lambda_f R]^{1/2} \tag{9.42}$$

Similarly, the radius of the mth dark ring is

[dark ring] $$x_m = (m\lambda_f R)^{1/2} \tag{9.43}$$

If the two pieces of glass are in good contact (no dust), the central fringe at that point ($x_0 = 0$) will clearly be a minimum in irradiance, an understandable result since d goes to zero at that point. In transmitted light, the observed pattern will be the complement of the reflected one discussed above, so that the center will now appear bright.

Newton's rings, which are Fizeau fringes, can be distinguished from the circular pattern of Haidinger's fringes by the manner in which the diameters of the rings vary with the order m. The central region in the Haidinger pattern corresponds to the maximum value of m (Problem 9.27), whereas just the opposite applies to Newton's rings.

An optical shop, in the business of making lenses, will have a set of precision spherical test plates or gauges. A designer can specify the surface accuracy of a new lens in terms of the number and regularity of the Newton rings that will be seen with a particular test gauge. The use of test plates in the manufacture of high-quality lenses, however, is giving way to far more sophisticated techniques involving laser interferometers (Section 9.8.2).

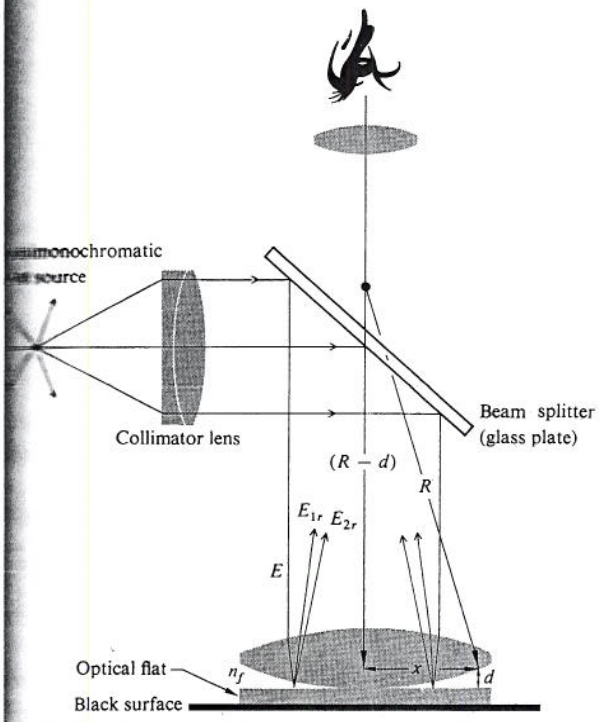

URE 9.26 A standard setup to observe Newton's rings.

9.4.2 Mirrored Interferometers

There are a good number of amplitude-splitting interferometers that utilize arrangements of mirrors and beamsplitters. By far the best known and historically the most important of these is the **Michelson Interferometer**. Its configuration is illustrated in Fig. 9.27. An extended source (e.g., a diffusing ground-glass plate illuminated by a discharge lamp) emits a wave, part of which travels to the right. The beamsplitter at O divides the wave into two, one segment traveling to the right

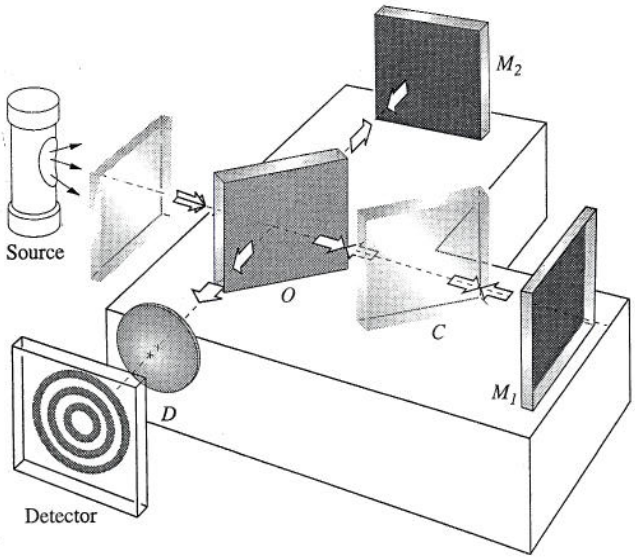

(a)

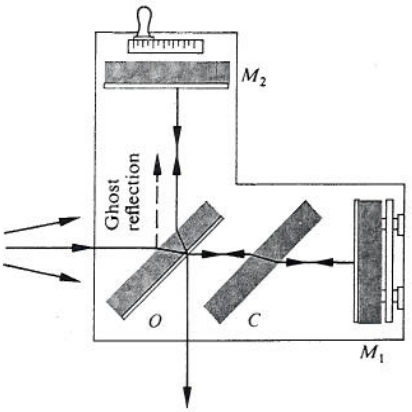

(b)

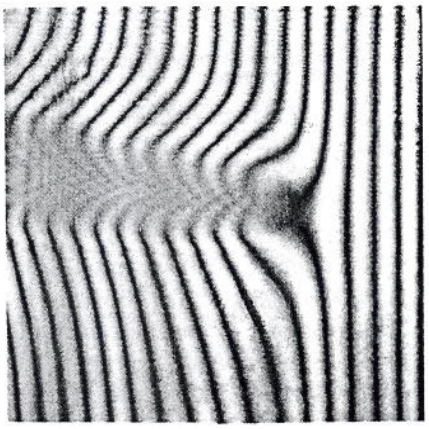

(c)

FIGURE 9.27 The Michelson Interferometer. (*a*) Circular fringes are centered on the lens. (*b*) Top view of the interferometer showing the path of the light. (*c*) A wedge fringe pattern was distorted when the tip of a hot soldering iron was placed in one arm. Observe the interesting perceptual phenomenon whereby the region corresponding to the iron's tip appears faintly yellow. (E. H.)

and one up into the background. The two waves are reflected by mirrors M_1 and M_2 and return to the beamsplitter. Part of the wave coming from M_2 passes through the beamsplitter going downward, and part of the wave coming from M_1 is deflected by the beamsplitter toward the detector. The two waves are united, and interference can be expected.

Notice that one beam passes through O three times, whereas the other traverses it only once. Consequently, each beam will pass through equal thicknesses of glass only when a *compensator plate* C is inserted in the arm OM_1. The compensator is an exact duplicate of the beamsplitter, with the exception of any possible silvering or thin film coating on the beamsplitter. It is positioned at an angle of 45°, so that O and C are parallel to each other. With the compensator in place, any optical path difference arises from the actual path difference. In addition, because of the dispersion of the beamsplitter, the optical path is a function of λ. Accordingly, for quantitative work, the interferometer without the compensator plate can be used only with a quasimonochromatic source. The inclusion of a compensator negates the effect of dispersion, so that even a source with a very broad bandwidth will generate discernible fringes.

To understand how fringes are formed, refer to the construction shown in Fig. 9.28, where the physical components are represented more as mathematical surfaces. An observer at the position of the detector will simultaneously see both mirrors M_1 and M_2 along with the source Σ in the beamsplitter. We can redraw the interferometer as if all the elements were in a straight line. Here M_1' corresponds to the image of mirror M_1 in the beamsplitter, and Σ has been swung over in line with O and M_2. The positions of these elements in the diagram depend on their relative distances from O (e.g., M_1' can be in front of, behind, or coincident with M_2 and can even pass through it). The surfaces Σ_1 and Σ_2 are the images of the source Σ in mirrors M_1 and M_2, respectively. Now consider a single point S on the source emitting light in all directions; let's follow the course of one emerging ray. In actuality a wave from S will be split at O, and its segments will thereafter be reflected by M_1 and M_2. In our schematic diagram we represent this by reflecting the ray off both M_2 and M_1'. To an observer at D, the two reflected rays will appear to have come from the image points S_1 and S_2 [note that all rays shown in (*a*) and (*b*) of Fig. 9.28 share a common plane-of-incidence]. For all practical purposes, S_1 and S_2 are coherent point sources, and we can anticipate a flux-density distribution obeying Eq. (9.14).

As the figure shows, the optical path difference for these rays is nearly $2d \cos \theta$, which represents a phase difference of $k_0 2d \cos \theta$. There is an additional phase term arising from the fact that the wave traversing the arm OM_2 is internally reflected in the beamsplitter, whereas the OM_1-wave is externally reflected at O. If the beamsplitter is simply an uncoated glass plate, the relative phase shift resulting from the two reflections

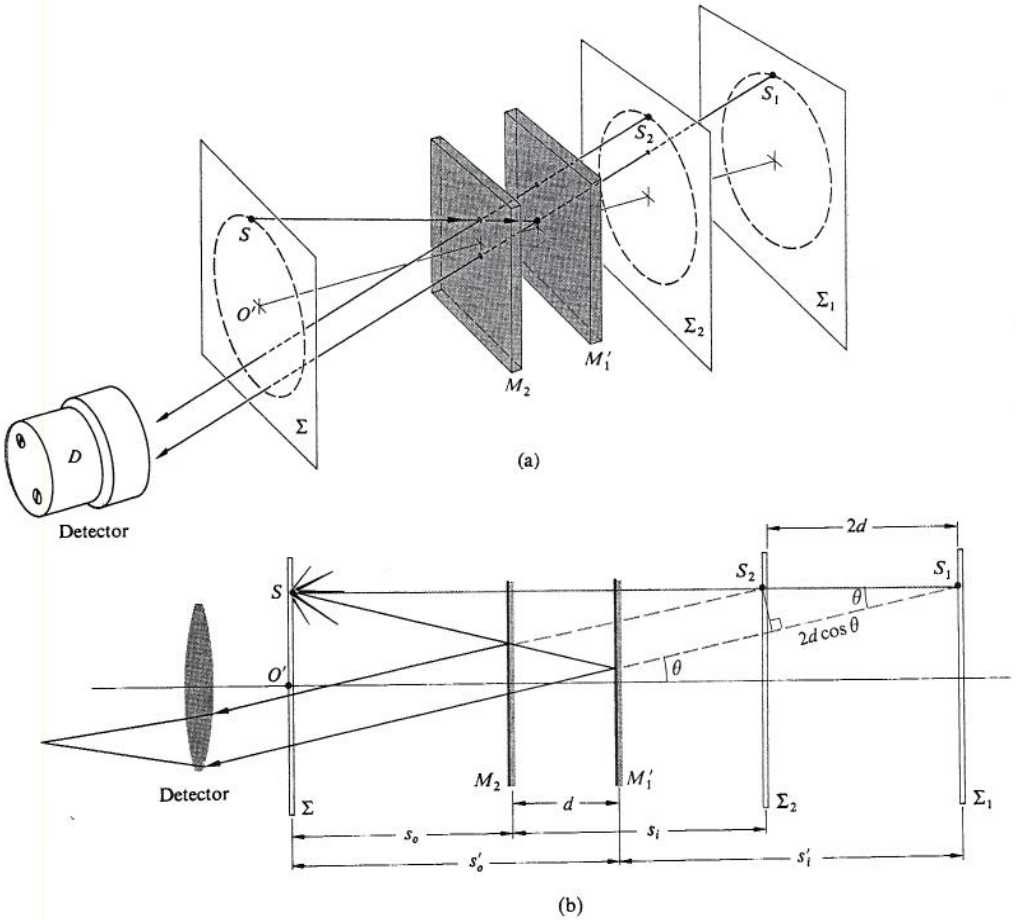

FIGURE 9.28 A conceptual rearrangement of the Michelson Interferometer.

will be π radians. *Destructive*, rather than constructive, interference will then exist when

$$2d \cos \theta_m = m\lambda_0 \tag{9.44}$$

where m is an integer. If this condition is fulfilled for the point S, then it will be equally well fulfilled for any point on Σ that lies on the circle of radius $O'S$, where O' is located on the axis of the detector. As illustrated in Fig. 9.29, an observer will see a circular fringe system concentric with the central axis of her eye's lens. Because of the small aperture of the eye, the observer will not be able to see the entire pattern without the use of a large lens near the beamsplitter to collect most of the emergent light.

If we use a source containing a number of frequency components (e.g., a mercury discharge lamp), the dependence of θ_m on λ_0 in Eq. (9.44) requires that each such component generate a fringe system of its own. Note, too, that since $2d \cos \theta_m$ must be less than the coherence length of the source, it follows that laser light will be particularly easy to use in demonstrating the interferometer (see Section 9.5). This point would be made strikingly evident were we to compare the fringes produced by laser light with those generated by "white" light from an ordinary tungsten bulb or a candle. In the latter case, the path difference must be very nearly zero, if we are to see any fringes at all, whereas in the former instance a difference of 10 cm has little noticeable effect.

An interference pattern in quasimonochromatic light typically consists of a large number of alternatively bright and dark rings. A particular ring corresponds to a fixed *order* m. As M_2 is moved toward M_1', d decreases, and according to Eq. (9.44), $\cos \theta_m$ increases while θ_m therefore decreases. The rings shrink toward the center, with the highest-order one disappearing whenever d decreases by $\lambda_0/2$. Each remaining ring broadens as more and more fringes vanish at the center, until only a few fill the whole screen. By the time $d = 0$ has been reached, the central fringe will have spread out, filling the entire field of view. With a phase shift of π resulting from reflection off the beamsplitter, the whole screen will then be an interference minimum. (Lack of perfection in the optical elements can render this unobservable.) Moving M_2 still farther causes the fringes to reappear at the center and move outward.

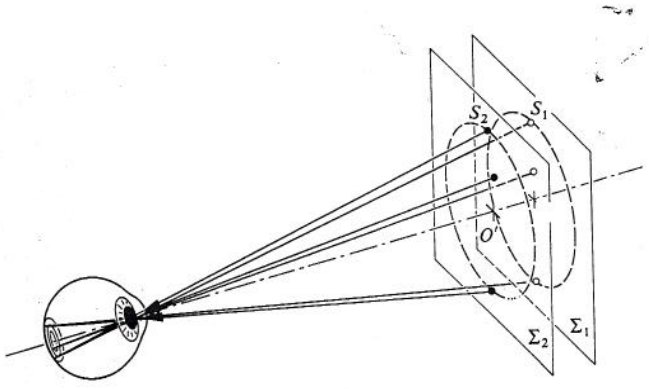

FIGURE 9.29 Formation of circular fringes.

Notice that a central dark fringe for which $\theta_m = 0$ in Eq. (9.44) can be represented by

$$2d = m_0\lambda_0 \tag{9.45}$$

(Keep in mind that this is a special case. The central region might correspond to neither a maximum nor a minimum.) Even if d is 10 cm, which is fairly modest in laser light, and $\lambda_0 = 500$ nm, m_0 will be quite large, namely 400 000. At a fixed value of d, successive dark rings will satisfy the expressions

$$\begin{aligned} 2d \cos \theta_1 &= (m_0 - 1)\lambda_0 \\ 2d \cos \theta_2 &= (m_0 - 2)\lambda_0 \\ &\vdots \\ 2d \cos \theta_p &= (m_0 - p)\lambda_0 \end{aligned} \tag{9.46}$$

The angular position of any ring, for example, the pth ring, is determined by combining Eqs. (9.45) and (9.46) to yield

$$2d(1 - \cos \theta_p) = p\lambda_0 \tag{9.47}$$

Since $\theta_m \equiv \theta_p$, both are just the half-angle subtended at the detector by the particular ring, and since $m = m_0 - p$, Eq. (9.47) is equivalent to Eq. (9.44). The new form is somewhat more convenient, since (using the same example as above) with $d = 10$ cm, the sixth dark ring can be specified by stating that $p = 6$, or in terms of the *order* of the pth ring, that $m = 399\,994$. If θ_p is small,

$$\cos \theta_p = 1 - \frac{\theta_p^2}{2}$$

and Eq. (9.47) yields

$$\theta_p = \left(\frac{p\lambda_0}{d}\right)^{1/2} \tag{9.48}$$

for the angular radius of the pth fringe.

The construction of Fig. 9.28 represents one possible configuration, the one in which we consider only pairs of parallel emerging rays. Since these rays do not actually meet, they cannot form an image without a condensing lens of some sort. Indeed, that lens is most often provided by the observer's eye focused at infinity. The resulting *fringes of equal inclination* (θ_m = constant) located at infinity are also *Haidinger fringes*. A comparison of Figs. 9.28*b* and 9.3*a*, both showing two coherent point sources, suggests that in addition to these (virtual) fringes at infinity, there might also be (real) fringes formed by converging rays. These fringes do in fact exist. Hence, if you illuminate the interferometer with a *broad source* and shield out all extraneous light, you can easily see the projected pattern on a screen in a darkened room (see Section 9.5). The fringes will appear in the space in front of the interferometer (i.e., where the detector is shown), and their size will increase with increasing distance from the beamsplitter. We will consider the (real) fringes arising from point-source illumination a little later on.

When the mirrors of the interferometer are inclined with respect to each other, making a small angle (i.e., when M_1 and M_2 are not quite perpendicular), *Fizeau fringes* are observed. The resultant wedge-shaped air film between M_2 and M_1' creates a pattern of straight parallel fringes. The interfering rays appear to diverge from a point behind the mirrors. The eye would have to focus on this point in order to make these *localized fringes* observable. It can be shown analytically* that by appropriate adjustment of the orientation of the mirrors M_1 and M_2, fringes can be produced that are straight, circular, elliptical, parabolic, or hyperbolic—this holds as well for the real and virtual fringes.

The Michelson Interferometer can be used to make extremely accurate length measurements. As the moveable mirror is displaced by $\lambda_0/2$, each fringe will move to the position previously occupied by an adjacent fringe. Using a microscope arrangement, one need only count the number of fringes N, or portions thereof, that have moved past a reference point to determine the distance traveled by the mirror Δd, that is,

$$\Delta d = N(\lambda_0/2)$$

Nowadays this can be done fairly easily by electronic means. Michelson used the method to measure the number of wavelengths of the red cadmium line corresponding to the standard meter in Sévres near Paris.†

The Michelson Interferometer can be used along with a few polaroid filters to verify the Fresnel–Arago Laws. A polarizer inserted in each arm will allow the optical path length difference to remain fairly constant, while the vector field directions of the two beams are easily changed.

A microwave Michelson Interferometer can be constructed with sheet-metal mirrors and a chicken-wire beamsplitter. With the detector located at the central fringe, it can easily measure shifts from maxima to minima as one of the mirrors is moved, thereby determining λ. A few sheets of plywood, plastic, or glass inserted in one arm will change the central fringe. Counting the number of fringe shifts yields a value for the index of refraction, and from that we can compute the dielectric constant of the material.

The **Mach–Zehnder Interferometer** is another amplitude-splitting device. As shown in Fig. 9.30, it consists of two beamsplitters and two totally reflecting mirrors. The two waves within the apparatus travel along separate paths. A difference between the optical paths can be introduced by a slight tilt of one of the beamsplitters. Since the two paths are separated, the interferometer is relatively difficult to align. For the

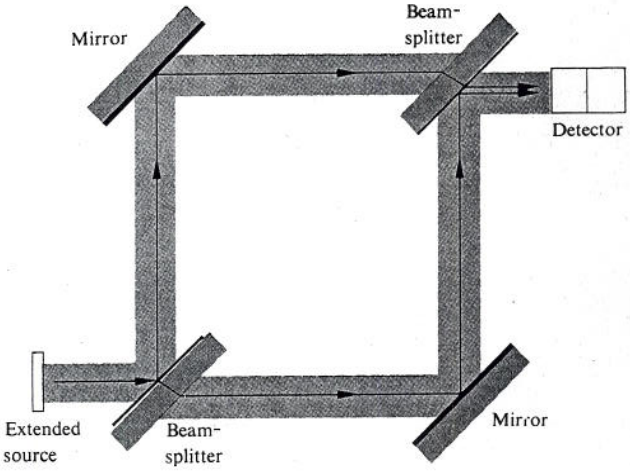

FIGURE 9.30 The Mach–Zehnder Interferometer.

*See, for example, Valasek, *Optics*, p. 135.

†A discussion of the procedure he used to avoid counting the 3 106 327 fringes directly can be found in Strong, *Concepts of Classical Optics*, p. 238, or Williams, *Applications of Interferometry*, p. 51.